Polarimetric Observations of Prescribed Bushfires in South Australia using an X-Band Phased Array Radar

Robert A. Palumbo, Eric J. Knapp, David J. McLaughlin, Stephen J. Frasier

University of Massachusetts, Amherst, Massachusetts, USA

Waddah A. Al-Ashwal, Douglas Gray

University of Adelaide, Adelaide, South Australia, Australia

Bradley Ferguson, Christopher P. McCarroll

Raytheon Company, Tewksbury, Massachusetts, USA

ABSTRACT

Wildfires in Australia, commonly bushfires, are a natural part of the country's ecosystem and help to clean out and recycle the local flora. During April and May of 2013, an X-Band Phased Array Radar was deployed to South Australia where it made polarimetric observations of eight prescribed bushfires conducted within and around the Adelaide Hills region. At each prescribed burn, the radar nominally performed fixed-elevation azimuth scans, as well as intermittent RHI (Range-Height Indicator) and volume scans, during the entire evolution of the burn. Narrow bandwidth (50 m range resolution) and high bandwidth (7 m range resolution) waveforms were alternately transmitted throughout each burn. Time-synchronized photography was also collected to document visual observations throughout. This talk presents measurements and polarimetric products observed from the prescribed bushfires. Copolar correlation coefficient within the plume is observed to be somewhat low, consistent with lofted debris particles. Doppler velocity measurements and time-synchronized photography show the rotation of the smoke plume, and the measured radar moments show patterns which distinguish localized areas above fire sources from particle drift amidst ground-level winds. Rapid azimuth scanning indicates the velocity of ambient ground winds, confirmed against local in situ measurements near the burn sites. These measurements provide a real-time evolution of the smoke plume dynamics at a spatial and temporal resolution that has never been observed with an X-band radar.

1. Introduction

Dry summer months and high ground winds create a high risk of uncontrolled wildfires in Australia. These bushfires can spread quickly in varying terrains and can change direction with shifts in local ambient winds. Understanding the fire morphology and relaying that information to local firefighters is crucial in avoiding loss of life and property.

A number of studies using remote sensing techniques to measure wild fire smoke and ash plumes have been performed. Banta et al. (1992) used an X-band Doppler radar to measure reflectivities from a forest fire near Boulder, Colorado having reflectivities as high as 10 to 20 dBZ within the smoke plume and 0 dBZ at an altitude of 10 km. Jones and Christopher (2010) analyzed S-band radar data and satellite imagery to observe a smoke and debris plume extending 100 km in range, with reflectivies near 20 dBZ at 5 km in height. Melnikov et al. (2009) also studied the polarization characteristics from these fires. He noted large, positive differential reflectivity, low copolar correlation coefficient, and high variances associated with differential phase and reflectivity measurements. Work has also been published on the use of LIDARs and higher frequency microwave radars for smoke particulate and ash plume observations (Tsai et al. 2009), and other studies have been performed to measure the radar cross section of forest fire particulate and debris matter (Ghorbani et al. 2012; Baum et al. 2012).

This paper presents polarimetric observations and analysis from a series of prescribed burns conducted in and around the Adelaide Hills region of South Australia. The data presented herein provides insight into the scattering mechanism and polarimetric properties of ash and debris plume particles at X-band.

2. Test Methodology

During April to May 2013, an X-band phased array radar system (Palumbo et al. 2012) made observations at seven prescribed bushfires in South Australia. One of the bushfires attended was an uncontrolled wildfire near the town of Cherryville, while the rest were controlled bushfires conducted by County Fire Service (CFS), Department of Environmental, Water and Natural Resource (DEWNR), and ForestrySA personnel. At each planned burn, the radar collected data from ignition through burn completion. To maximize radar sensitivity and cross range resolution of the smoke observations, the radar was located less than 2 km in range from the onset of the burn location, with boresight of the antenna directed towards the center of the burn site.

The radar made polarimetric (ATAR, Alternate Transmit, Alternate Receive) measurements at a fixed pulse repetition frequency of 3 kHz. Three waveforms were used intermittently during each burn, having range resolutions of 50 m, 15 m, and 7 m. Dwell times for each azimuthal radial were varied from 20 ms to 350 ms, with the radar nominally operating at a 40 ms dwell. The radar scanned at fixed elevations across a 90° sector, with intermittent RHI (Range-Height Indicator) and volumetric scans executed when the smoke plume intensity peaked. Clutter maps were also taken before and after each burn to be used as ground truth for comparative purposes.

Mobile weather stations provided local in situ measurements of the ambient environmental conditions near the burn (less than 1 km from the burn site) for the uncontrolled bushfires and several of the larger prescribed burns. These provide up-to-date temperature, pressure, humidity, and wind velocity measurements. In addition, a camera mounted on the top of the radar system collected snapshots of the radar field-of-view, time synchronized with every azimuth scan collected.

3. Observations

a. Scattering Mechanism

Measurements of fallen ash and debris made at a prescribed burn at the Belair Conservation Park (05 April) show that large debris particles consisted of either plate-like, leaf ash or complex debris from burnt grass and scrub. Plate-like particle matter samples, identified as Eucalyptus, Gum Tree, or Bracken Fern leaves, measured between 5 cm and 15 cm along its horizontal plane and less than 1 cm in thickness. Grass and other scrub debris samples were a complex spheroidal shape filled with rough, jagged edges and clusters measuring axial radii between 5 cm and 10 cm. These measurements agree with past work performed. Banta et al. (1992) determined particles to have a "flat, needle-like" shape from Circular Depolarization Ratio Measurements, and Melnikov et al. (2009) modeled debris shape as spheroidal (either oblate or ellipsoidal) with an unknown rotation angle.

In addition to particle size and shape, the dielectric constant of scattering objects effects data returns. Baum et al. (2012) measured the complex dielectric constant at X-band (10 GHz) of several common types of Australia flora, having absorption coefficients as low as 0.32 for Bracken Fern ($\varepsilon = 4.85 + 0.51j$) or as high as 0.61 for Wattle Tree ($\varepsilon = 11.44 + 1.71j$). Eucalyptus tree, a common species in South Australia, has an absorption coefficient of 0.41 ($\varepsilon = 6.30 + 0.06j$). This variation in dielectric constants could create uncertainty in reflectivity measurements at each burn, as fuel load and forest density changes.

b. Observations

Figure 1 presents a snapshot of data at 15:44 local time (06:14 UTC) during the Cherryville uncontrolled bushfire (10-May-2013). Figure 1(a) shows the rising column of white smoke between 100 and 400 m cross range, which correlates to an area of increased reflectivity in fig. 1(b). Towards the right side of the photo, the smoke seems to disperse and become darker gray in color. The arrows in fig. 1(b) indicate the radar heading and current wind direction, showing that the smoke plume motion and direction is dominated by ambient ground winds.

Comparison between fig. 1(b) and fig. 1(d) indicates correlation between higher reflectivity and lower differential reflectivity. Mean Z_{DR} near (0.2 km, 2.0 km) (cross range, down range) is 2.19 dB ($\sigma = 0.55$ dB), while the mean value at (0.9 km, 2.2 km) is 2.90 dB ($\sigma = 1.00$). Another patch of reduced differential reflectivity can also be seen at (1.1 km, 2.2 km). Copolar correlation coefficient in fig. 1(e) shows no recognizable pattern or correlation with the fire source, with a mean value near 0.4 within the smoke plume.

Figure 2 shows normalized distributions of differential reflectivity and copolar correlation coefficient for two prescribed burns and one uncontrolled bushfire. Data is thresholded at 10 dB Signal-to-Noise Ratio (SNR) to mitigate noise bias. Shown in fig. 2(a) for three burns, average differential reflectivity is between 1 to 2 dB for each prescribed burn and uncontrolled bushfire observed. Positive Z_{DR} is consistent with previous work (Melnikov et al. 2009) and agrees with debris sample measurements as predominantly flat, plate-like particles from leaf matter. However, the mean value and variation of differential reflectivity is reduced in areas above fire sources, compared with areas upwind.

Copolar correlation coefficient was low throughout the burns, averaging between 0.4 and 0.7. Figure 2(b) shows the distribution of ρ_{hv} during three observed fires. Mean correlation coefficient during the prescribed burns, Barossa Valley and Cox Scrub, is much higher than that reported in the uncontrolled bushfire at Cherryville. The uncon-

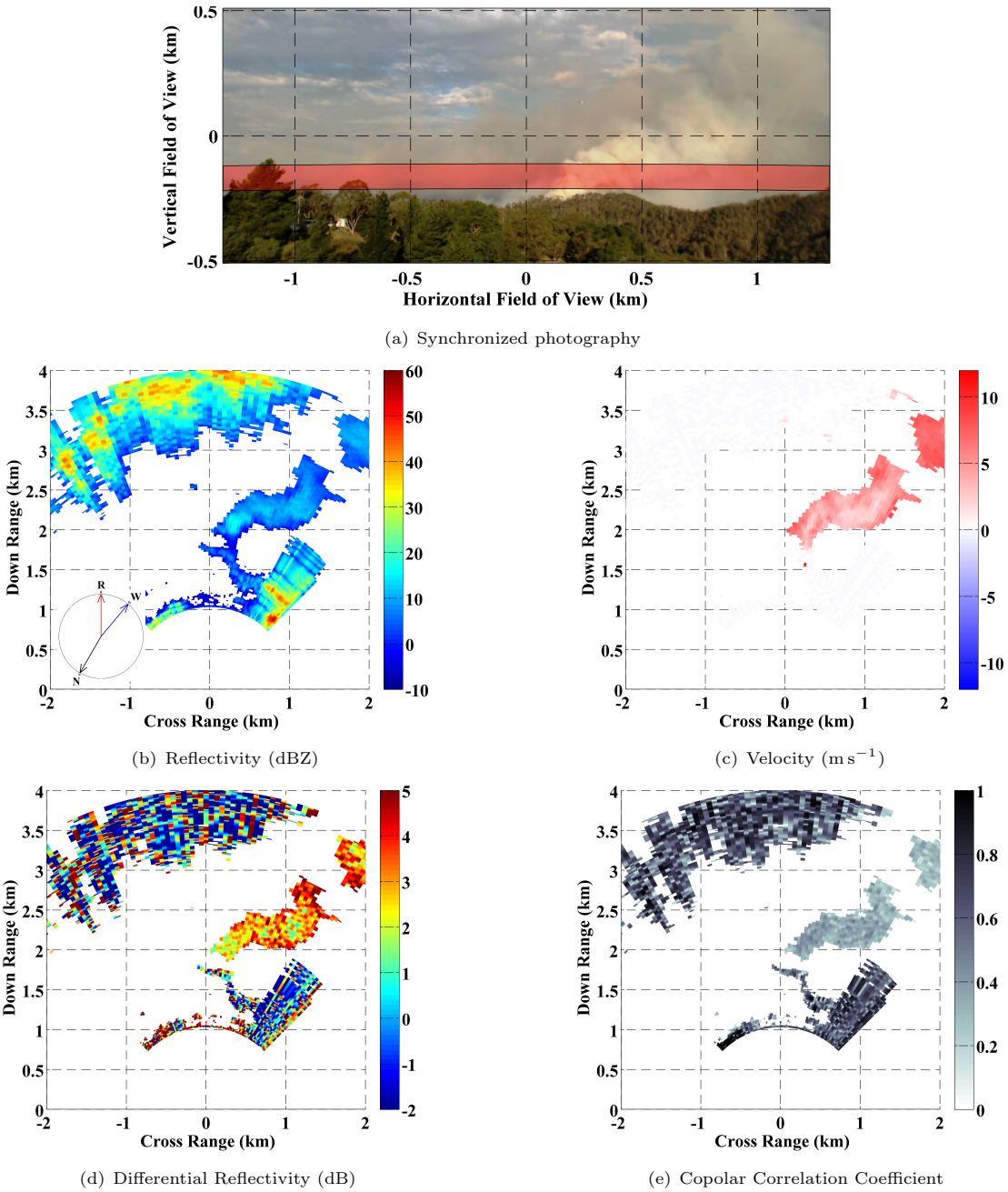

(a) Synchronized photography

(b) Reflectivity (dBZ)

(c) Velocity ($\mathrm{m\,s^{-1}}$)

(d) Differential Reflectivity (dB)

(e) Copolar Correlation Coefficient

FIG. 1. Timelapse photography and data from the Cherryville, SA bushfire at 15:44 local time (06:14 UTC). From top are (a) synchronized photo, (b) reflectivity, (c) velocity, (d) differential reflectivity, and (e) copolar correlation coefficient. The red shaded area in (a) shows the radar field-of-view in the scene, using the radar3 dB elevation beamwidth (2.8°). The arrows in (b) indicate due North (N), the radar heading (R), and measured wind directions (W).

trolled bushfire was more intense than any of the prescribed burns, with measured reflectivities as high as 40 dBZ versus 25 dBZ for controlled burns. The increased heat flux may be causing the reduced correlation coefficient in the uncontrolled fire observed. Mobile weather station data and fuel load measurements are still being analyzed to determine the root cause of this difference.

c. Analysis

We hypothesize that the localized variations in Z_{DR} in fig. 1(d) are due to differences in the motion of ash and debris particles around fire sources. Above the fire source, where the heat flux and vertical updraft within the convection column are highest, the particles tumble more quickly about their axis as they are propelled upwards. As they

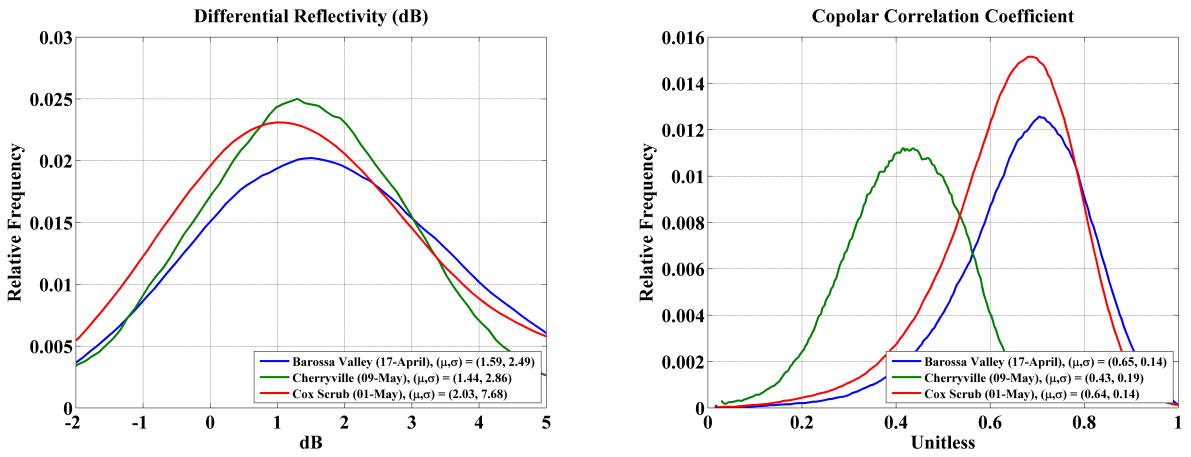

(a) (b)

FIG. 2. Collected statistics of (a) differential reflectivity and (b) copolar correlation coefficient measurements from three observed bushfires.

interact with ground winds and are pushed away from the fire, particles tend to float or drift with their major axis parallel to the ground.

Initial analysis of the data shows no recognizable pattern in ρ_{hv}, either at the fire source or areas downwind. While some results indicate localized high values (> 0.9), it is inconclusive if these are simply statistical fluctuation. Studies and field work (Radke et al. 1991) have observed that intense fires can create a downdraft of mist or water droplets, formed by water condensation onto smoke particulates as warm, moist air from the convective column cools and falls. This suggests that ρ_{hv} during these types of fires may be higher and more resembling precipitation. It is unclear as to whether the fires observed were not intense enough to create this effect, or the mixture of condensed water droplets and larger ash particles would still reduce the copolar correlation coefficient within the plume.

The largest plume radial extent observed was less than 1 km, while most were less than 500 m. This made it difficult to estimate specific differential phase (K_{DP}) for the datasets. However, data shows high local variation of Φ_{DP}, between 10° to 20° within a 50 m range span, which indicates large backscatter differential phase. This is either caused by a high complex dielectric constant of scatterers, as noted previously, or Mie scattering from the much larger debris matter reported earlier.

4. Conclusion

In this paper, X-band polarimetric observations were presented from a series of prescribed burns conducted in South Australia, and results were compared against an observed uncontrolled bushfire. Increased reflectivity and spectral width was observed at the fire sources, compared against time-synchronized photography. Results indicate positive differential reflectivity, indicative of flat, ellipsoidal particles and low copolar correlation coefficient, consistent with previous work. Also noted was a dependence between differential reflectivity and reflectivity, with data showing lower Z_{DR} in areas of increased reflectivity. Differential phase measurements show large backscatter differential phase through the debris plume.

REFERENCES

Banta, R., L. Olivier, E. Holloway, R. Kropfli, B. Bartram, R. Cupp, and M. Post, 1992: Smoke-column observations from two forest fires using doppler lidar and doppler radar. *Journal of Applied Meteorology*, **31**, 1328–1349.

Baum, T., L. Thompson, and K. Ghorbani, 2012: A complex dielectric mixing law model for forest fire ash particulates. **9 (5)**, 832–835.

Ghorbani, K., T. C. Baum, and L. Thompson, 2012: Properties and radar cross-section of forest fire ash particles at millimeter wave. *The 42nd European Microwave Conference (EuMC'12)*, 1335–1338.

Jones, T. and S. Christopher, 2010: Satellite and radar remote sensing of southern plains grass fires: a case study. *Journal of Applied Meteorology and Climatology*, **49 (10)**, 2133–2146.

Melnikov, V., D. Zrnic, R. Rabin, B. Pierce, and P. Zhang, 2009: Radar polarimetric signatures of fire plumes. *Proc. 25th Conference on International Interactive Information and Processing Systems.*

Palumbo, R. A., E. Knapp, K. Wood, and D. J. McLaughlin, 2012: Deployment considerations and hardware technologies for realizing X-Band radar networks. *Proc. The*

Seventh European Conference on Radar In Meteorology and Hydrology (ERAD'12).

Radke, L. F., et al., 1991: Particulate and trace gas emissions from large biomass fires in north america. *Global Biomass Burning: Atmospheric Climatic and Biospheric Implications*.

Tsai, P., S. Frasier, S. Goodrick, G. Achtemeier, and M. Odman, 2009: Combined lidar and radar observations of smoke plumes from prescribed burns. *Proc. The Fourth Symposium on LiDAR Atmospheric Applications*, 10–16.